Effect of Cd/Te Ratio on the Formation of CdTe Magic-Sized Quantum Dots during Aggregation†

Pinar Dagtepe and Viktor Chikan*

Kansas State University, Department of Chemistry, Manhattan, Kansas 66506-3701

Received: March 14, 2008; Revised Manuscript Received: August 15, 2008

In this study, the aggregation dynamics of magic-sized CdTe quantum dots is investigated. The experiments show that the growth kinetics of the quantum dots is very sensitive to the Cd/Te ratio. The crossover from tellurium-rich to cadmium-rich conditions produces a very different aggregation pattern, which can be explained by the lack of formation of magic-sized nanoparticles during the reaction conditions. A simple simulation that includes both monomer-induced growth and aggregation growth is presented to reproduce the experimentally observed aggregation patterns. The simulation results strongly suggest that the experimental aggregation pattern can be reproduced if initially a double magic-sized distribution is assumed. The numerical data clearly show that the aggregation is enhanced by the dipole−dipole interaction. Simulations also suggest that the neck formation of the CdTe quantum dot aggregates is unlikely under the experimental conditions. The absence of neck formation is in agreement with the expectations during high-temperature synthesis.

Introduction

Controlling the growth of semiconductor nanoparticles (NP) is important for technology to produce materials with well-defined properties.[1] One of the main research efforts of the nanoparticle scientific community has been to create highly crystalline nanomaterials.[2] From this point of view, the aggregation of nanoparticles is an undesirable mechanism for the formation of nanoparticles because it leads to the formation of crystal defects. However, if the aggregation of nanoparticles can be controlled,[3] then the solution-phase self-assembly of materials can be better understood and utilized to create novel materials with well-defined defects.

The growth of nanoparticles can be thought of as a simple crystal growth problem. During crystal growth, the first step is the formation of nuclei from a supersaturated solution. Supersaturation can be achieved by changing the thermodynamic properties of the solution (1) by the fast decomposition of precursor molecules, (2) by decrease the temperature, or (3) by a combination of the two. The initial formation of small nuclei is followed by the slow growth of nanoparticles separated from the nucleation step. According to the accepted model, the nanoparticle growth is mainly controlled by the Gibbs−Thompson effect. The Gibbs−Thomson effect predicts that particles with larger curvature exhibit higher effective monomer solubility, which is mainly responsible for the deviation from the simple crystal growth problem. An elegant numerical method proposed by Talapin at al[4] shows that at high monomer concentrations the initial particle size distribution undergoes focusing as observed experimentally by many research groups.[5] The model also shows that once the monomer concentration drops, the particle distribution will defocus, which is the well-known Ostwald ripening process.[6] The nanoparticle system as a whole is heading toward the thermodynamic minimum by decreasing the surface area and forming more bulklike particles with more flat surfaces. The model assumes that particles can get larger only by exchanging monomers with the solution and consequently with each other.

Alternatively, a nanoparticle system can minimize its overall energy by aggregation, when two particles come into close contact and form a new particle with a volume that is the sum of the constituents. There are attractive and repulsive forces involved in the aggregation, which control the observed aggregation kinetics. If repulsive forces dominate the particle−particle interaction, then aggregation does not take place on the time scale of observation. The interactions can have strong van der Waals character, as in the case of the aggregation of GaSe nanodisks.[7] The interaction of GaSe nanodisks is also increased by the larger interaction surfaces, which are absent in the case of spherical nanoparticles. Electrostatic interaction leads to the aggregation of spherical nanoparticles, as can be observed in solutions containing silver and gold nanoparticles.[8,9] When the attractive forces are deliberately tailored by using cross-linking molecules, the aggregation can lead to nanoparticle-based aggregates with novel properties.[10,11]

A specific example of aggregated growth that has attracted some attention is the oriented attachment of semiconductor nanoparticles to form nanowires. In oriented attachment (OA), nanoparticles attach and organize themselves along the same crystallographic axis via directional dipole−dipole interaction. The proposed reason for the OA has been attributed to the presence of a net dipole moment in the crystal.[12,13] Interestingly, the presence of a net dipole is not limited to polar crystals but may be the result of defects.[13] The typical orientation of dipoles is a head-to-tail arrangement when there is significant attraction between particles. As a result of the OA of *n* spherical NPs, nanowires will be formed with a length approximately *n* times the diameter of the nanoparticles. In the literature, there are many examples of the oriented attachment of nanoparticles, including ZnS,[14] CdTe,[15,12] ZnTe,[16] PbSe,[17] and CdS nanoparticles. In the study of PbSe, nanowires are synthesized, and the attachment of nanoparticles is through identical crystal faces leading to OA. A recent simulation model explains the formation of nanorods from quantum dots due to OA, predicting the length distribution of the nanorods.[14] Although the examples of oriented attachment

† Part of the "Stephen R. Leone Festschrift".

* Author to whom all correspondence should be addressed. E-mail: chikan@ksu.edu.

10.1021/jp802254n CCC: $40.75
Published on Web 09/05/2008

leading to nanowire formation are numerous, not all of the nanoparticle aggregation will yield nanowires, especially at higher temperatures when nanowires can collapse.

In one aggregation mechanism, the nanoparticle aggregates may undergo a complete phase transformation and collapse, resulting in a "new" particle. Another possibility for the mechanism of aggregation is that the aggregated nanoparticles will form a neck, which accelerates the growth of the nanoparticle aggregate via monomer exchange as observed experimentally during the fusion of nanoparticles into nanowires.[16−19] This later aggregation mechanism will result in particles with volumes larger than the volumes of their original constituents. Therefore, the two mechanisms can be differentiated by experimental methods that can sensitively measure volume change during nanoparticle growth.

There are an increasing number of reports on nanoparticle synthesis showing that multiple sizes of nanoparticles may coexist in solution.[20,21] Our previous report[22] has shown that magic-sized CdTe nanoparticles aggregate in a high-temperature coordinating solvent, which results in variously sized nanoparticle aggregates as a function of time. However, no experimental control is given over the observed aggregation pattern. In fact, varying the solvent composition and temperature over a wide range yielded a very similar aggregation pattern. In this work, the varying ratio of Cd and Te results in a very different aggregation pattern as a result of the stabilization or destabilization of magic-sized CdTe nanoparticles. To reproduce the observed aggregation pattern, a simple simulation has been developed to include both monomer exchange and the aggregation-driven growth of the nanoparticles. The simulation shows good agreement with the experiment, considering the qualitative nature of the approach.

Experimental Section

Chemicals. Tellurium powder (99.999%), CdO (99.999%), phenylphosphonic acid (99%), trioctylphosphine (TOP, 97%), trioctylphosphine oxide (TOPO, 90%), 1-hexadecylamine (HDA, 90%), anhydrous methanol (99.8%), anhydrous toluene (99.8%), *n*-hexylphosphonic acid (HPA, 100%), octadecylamine (ODA, 98%), dodecylamine (DDA, +98%), stearic acid (purified), dimethylcadmium (97%) were used. TOPO, TOP, and HDA were purified by vacuum distillation.

Synthesis of CdTe Nanoparticles. The synthesis method and the experimental setup are identical to the those given in a previous publication.[22] The experimental setup allows us to obtain in situ absorption spectra at the synthesis temperature. The reaction conditions for preparing CdTe nanoparticles used in this experiment are as follows. A mixture of CdO (1 mmol) and HPA (5 mmol) is heated to approximately 300 °C to obtain a clear solution in a three-necked flask. The reaction mixture is cooled and kept under argon for approximately 24 h. Hexadecyl amine (8.5 g) and trioctyl phosphine oxide (TOP, 8.5 g) are added, and the temperature of the reaction vessel is increased to 200 °C until a homogeneous, optically clear solution is obtained. A solution (10 mL) containing tellurium (0.052 M) is injected to initiate the growth of the nanoparticles. The injection temperature is varied between 240 and 270 °C. After injection, the temperature of the hot solution drops by approximately 40 °C. At different stages of the synthesis, aliquots are removed to determine variously sized QDs while monitoring the UV−vis spectrum simultaneously. Cd/Te ratios are also changed, which are given as 1/0.5, 1/1, 1/5, and 1/10. During purification, the solution is washed several times with anhydrous methanol. The precipitate is then isolated by centrifugation and dried in a vacuum oven at room temperature. After the solvents are removed, the precipitate is dissolved in anhydrous toluene.

Results and Discussion

Controlling the self-assembly of quantum dots in solution is important in creating novel structures. A key challenge is to identify important parameters that could potentially manipulate the aggregation of quantum dots. The sequential aggregation of CdTe nanoparticles via the formation of magic-sized QDs has already been reported.[22] Figure 1 shows the in situ absorption spectra of CdTe QDs in sequence with different Cd/Te ratios. The spectra show the sequential appearance of relatively sharp peaks at high temperatures. The first sharp absorption peak corresponds to magic-sized nanoparticles appearing in the tellurium-rich reaction mixture at 240 °C. The kinetics of QD growth in solutions containing different Cd/Te ratios significantly varies. The spectra are taken 70, 152, 238, and 490 s after injection. At 70 s, all of the spectra have different features. In Figure 1a (Cd/Te 1:0.5), there is a flat line indicating neither nucleation nor particle growth. In Figure 1b, a similar feature can be seen. In Figure 1c,d, a sharp peak associated with the magic-sized CdTe QDs already starts forming. A similar trend can be noticed at later times in Figure 1a−d. Briefly, the increasing ratio of tellurium accelerates the growth of the CdTe particles. Qualitatively, the amount of absorbance also increases, which indicates that the number density of particles is greater as well. Another key difference among the various ratios of Cd/Te is that the Figure 1a data corresponding to cadmium-rich conditions does not show the appearance of magic-sized nanoparticles. The absence of magic-sized nanoparticles from the growth solution still does not mean that there is no aggregation of the quantum dots. In fact, the reduced crystallinity of the cadmium samples from XRD suggests otherwise.

Figure 2 presents the X-ray diffraction patterns of two samples with 1:1 and 1:0.5 Cd/Te ratios. The sample that has a 1:1 Cd/Te ratio has an identical pattern to that of the tellurium-rich samples; therefore, the XRD from the other samples is omitted. In Figure 2a, there are three XRD peaks centered at 2θ angles of ∼24, 40, and 47°. Figure 2b only shows one broad XRD peak at 23°. The tellurium-rich sample in Figure 2a indicates a more crystalline structure whereas in Figure 2b the cadmium-rich condition corresponds to a sample that is more amorphous. Although the size analysis of the nanoparticles indicates similar final distributions, the lack of the distinct peak in Figure 2b and the increased fwhm of the reflection suggest that the crystalline domains in the cadmium-rich samples are smaller. The Debye−Scherer method yields 3.7 ± 0.3 and 1.1 ± 0.2 nm domain sizes of the tellurium- and cadmium-rich samples, respectively. The positions of the peaks match the zinc blende CdTe QDs in Figure 2a, but the presence of a (101) peak at ∼26° is an indication of the phase transition from the zinc blende to wurtzite structure, as observed before.[27]

Figure 3 shows the absorption spectra of the very small 1.9 nm CdTe QDs (magic size). To obtain this size, the tellurium-rich reaction is quenched by injecting a large amount of TOP solvent to decrease the reaction temperature. In Figure 3, the ratio of Cd/Te in CdTe QDs is 1:5. The QD absorption peak indicates a very narrow size distribution with a spectral full width at half-maximum (fwhm) of 17 nm. The inset is the high-resolution transmission electron microscopy (HRTEM) image of the particles. This size is most likely identical to the ones observed by Rockenberger et al.[23] The observation of a narrow size distribution magic size is very important in these experi-

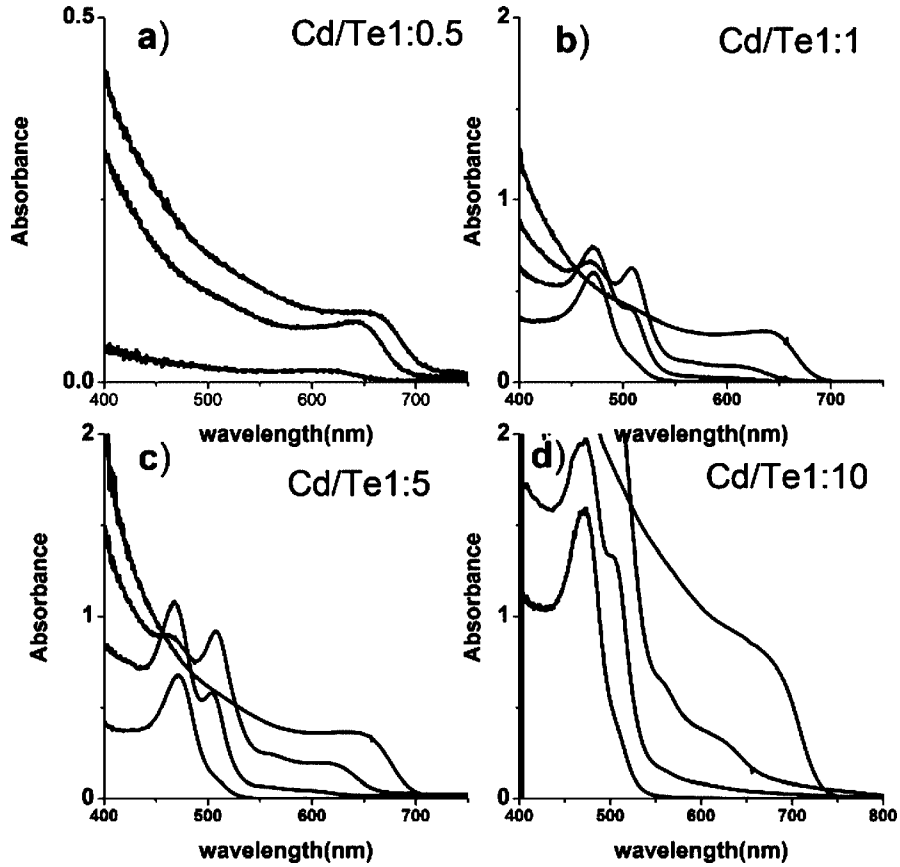

Figure 1. Variation of growth kinetics of CdTe nanoparticles with the CdTe ratio. Only the tellurium concentration is changed. The in situ absorption spectra are taken at 240 °C at the same times after injection (70, 152, 238, and 490 s). For the cadmium-rich condition, the inset shows different times to describe the early-time kinetics better. Notice the appearance of magic-sized nanoparticles for the tellurium-rich conditions.

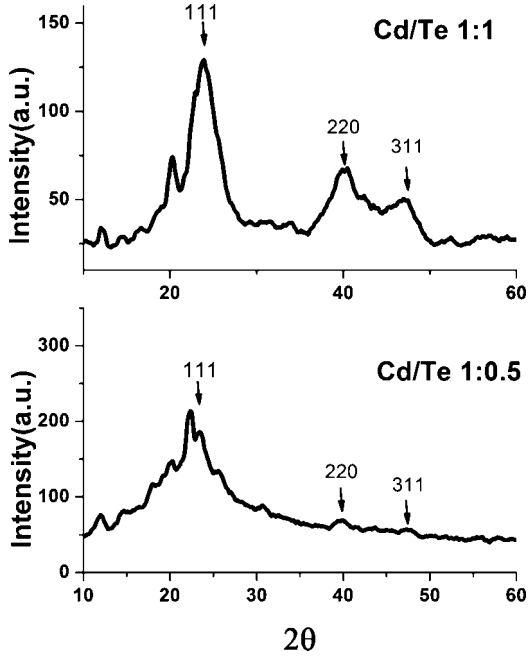

Figure 2. XRD pattern of the 1:1 and 1:0.5 Cd/Te initial ratio CdTe nanoparticles.

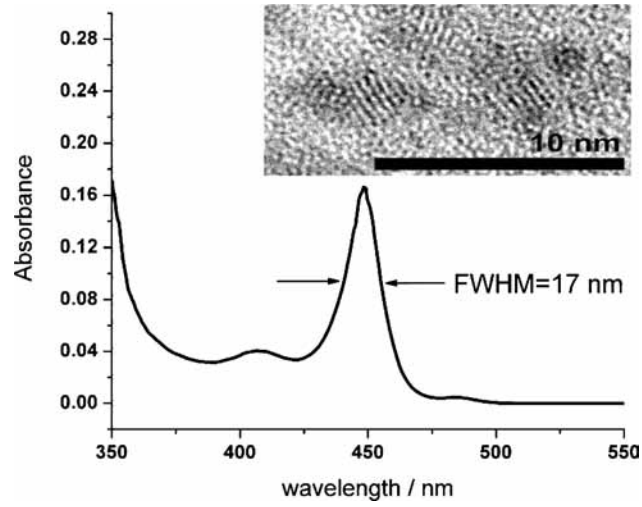

Figure 3. Absorption spectrum of the magic-sized CdTe nanoparticles. The inset shows the HRTEM image of the zinc blende structure of the magic-sized nanoparticles.

ments, which makes it possible to extract quantitative information about the aggregation dynamics. Several arguments exist as to why magic-sized quantum dots form. The two important ones worth mentioning assume thermodynamic reasoning. The realization of magic size can be the result of a closed-shell stable electronic structure.[24] Another reason for the large thermodynamic stability may originate from the delicate balance between the surface and the intrinsic energy of the nanoparticle.[25,26] Under Te-rich conditions, the small particles aggregate and form the larger ones. Various studies on the growth of CdTe nanowires from the oriented attachment of smaller particles suggest that the aggregation is driven by dipole−dipole interactions.[12,32] The small particles have a zinc blende crystal structure, but as they grow, they have the tendency to undergo a phase transition from zinc blende to wurtzite, as shown in the XRD pattern (Figure 2a).[22]

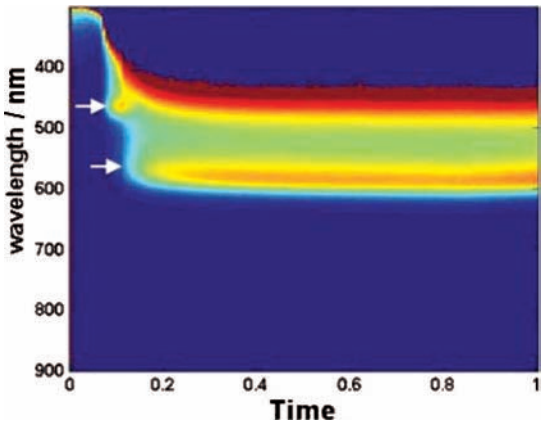

Figure 4. (A) Evolution of the in situ absorption spectra of the CdTe nanoparticles using Me_2Cd for the 2:1 Cd/Te ratio. The arrows indicate the appearance of sharp peaks corresponding to magic-sized nanoparticles.

In the next experiment, the CdO precursor is replaced by Me_2Cd. When the same amount of cadmium is used as in the case of the 1:5 Cd/Te ratio, the observed growth kinetics is very similar to the 1:0.5 Cd/Te ratios, which shows that there is a significant difference between the activity of the cadmium precursor and how it affects the growth kinetics. The lack of aggregation growth suggests that if the cadmium concentration is further increased no aggregation should be observed. Contrary to these expectations, as the cadmium concentration increases, the aggregation pattern returns as shown in Figure 4. Interestingly, only two definite sizes are observed, and the growth seems to stop, which is distinctly different from the aggregation mechanism described above. The first size is the same as the magic-sized nanoparticle, and the second observed size is approximately 2.5 ± 1.0 nm from TEM and 2.8 ± 0.2 nm on the basis of the sizing curve.[22] Qualitatively, the difference could be the result of the reactivity of the cadmium precursors. Whereas CdO is present in the solution and tellurium is injected, Me_2Cd needs to decompose first to supply the cadmium for the QD growth. In the initial phase of the decomposition, the conditions correspond to the tellurium-rich conditions, but when all the cadmium decomposes, the cadmium-rich condition stops further growth. These results are in agreement with the experimental observation for nanowire growth from oriented attachment. Deng et al. have found that under cadmium-rich conditions spherical growth is preferred whereas tellurium-rich conditions promote the linear assembly of CdTe nanoparticles.[27] The qualitative explanation of the stopped aggregation could be explained by the change in dipoles in the QDs under the reaction conditions. As will be shown in the simulation part, the presence or lack of a dipole moment in the nanoparticles may influence the rate of aggregation but does not explain the different aggregation patterns. In conclusion, when the conditions are cadmium-rich, no magic-sized nanoparticles are formed, but there the aggregation mechanism seems to be the dominant growth mechanism.[20]

The key question is why there is now magic-size formation under tellurium-rich conditions. The results strongly suggest that the magic-sized nanoparticle formation is driven by thermodynamic control of the system. Thermodynamic control of metal[28] (e.g., digestive ripening of gold nanoparticles in the presence of alkyl thiols) and semiconductor nanoparticles[29] is well documented in the literature. Briefly, the overall chemical potential (μ_{tot}) of the systems can be described by the following equation:

$$\mu_{tot} = \mu_{surf} + \mu_{bind} \quad (1)$$

The first term describes the increased surface energy (μ_{surf}) of the particles due to the Gibbs−Thomson effect. The second term (μ_{bind}) represent the term that will lower the overall chemical potential due to the binding of the surface ligands. When the two terms have different functional dependence on the size of the nanoparticles, the overall chemical potential will have a minimum at a given size. Interestingly, for perfectly spherical particles the argument will not work because both the surface energy and the binding energy scale the same way, resulting in no minimum in the overall chemical potential. These ideas translate into the CdTe system in a similar way. Under cadmium-rich conditions, the binding ligand is the hexyl phosphonic acid, which does not result in a minimum (or very broad minimum) in the overall chemical potential curve, which leads to relatively broad size distribution via thermodynamic control. When the conditions are tellurium-rich, the tellurium will act as a ligand, which produces a minimum in the overall chemical potential, corresponding to the above observed magic-sized CdTe nanoparticles. When various ligands are used under tellurium-rich conditions, the aggregation pattern remains almost identical, supporting this assumption. The above model is rather simplistic and ignores the details of the atomic and molecular structure of the nanoparticles and binding ligands. A more detailed understanding of the binding is expected from calculations.

Simulation of Aggregation Dynamics of Nanoparticles. To understand the aggregation dynamics of the nanoparticles better, a kinetic simulation is implemented. The goal of the simulation is to reproduce the experimentally observed aggregation pattern of the magic-sized CdTe nanoparticles and to verify whether the aggregated particles form a neck or undergo complete collapse and phase transformation. In other words, if a particle with volume$_1$ and another particle with volume$_2$ collide, then is the volume of the resulting particle the sum of the volumes of the colliding particles or is it larger? The simulation consist of two major parts: (1) the monomer-induced growth of the particles and (b) the aggregation of the nanoparticles. The monomer-induced growth is explained in detail by Talapin et al.[4] and by eq 2 in terms of dimensionless parameters, where $dr/d\tau$ is the size-dependent growth rate of nanoparticles, S is the monomer oversaturation, K is a dimensionless parameter describing whether the growth is reaction-controlled or diffusion-controlled, and α is the transfer coefficient. For this work, only the diffusion-controlled case is considered.

$$\frac{dr}{d\tau} = \frac{S - e^{1/r^*}}{r^* + Ke^{\alpha/r^*}} \quad (2)$$

First, the calculation of the rate of aggregation proceeds by calculation of the Brownian collision frequency of particles. The collision frequency (q) of particles i and j is

$$q(i, j) = 4\pi(D_i + D_j)(R_i + R_j) \quad (3)$$

where D_i is the size-dependent diffusion coefficient of particle i.

$$D_i = \frac{k_B T}{6\pi\mu R_i} \quad (4)$$

The aggregation of the particles is described by the Smoluchowski equation:[30,31]

$$\frac{dn_k}{dt} = \frac{1}{2}\sum_{i=1}^{k-1} q(k-1, i)n_{k-i}n_i - n_k\sum_{i=1}^{\infty} q(i, k)n_i \quad (5)$$

Here, dn/dt describes the population change of the kth particles due to the formation of new aggregates from smaller

TABLE 1

parameter	value
S	10/900
K	0.001 (diffusion-controlled)
μ	100 D[32]
monomer volume	4.1×10^{-5} mol/m^3 for CdTe
simulation volume	3×10^{-13} m^3
no. of particles	$(5-10) \times 10^3$
dt	$(2-20) \times 10^{-4}$
α	0.5
initial particle size	$R = 1.185$ and 0.812 nm
fwhm of distribution	0.03 and 0.3 nm
dt	$(2-20) \times 10^{-5}$ s
no. of steps	$(5-20) \times 10^3$

particles. To consider the effect of the increased aggregation rate due to the presence of the dipole−dipole interaction, the collision frequency is expressed as $q(i, j)/W$, where W describes the modification of the collision frequency due to the presence of a potential. W takes values between 0 and 1, thus increasing the collision frequency between particles when there is a strong interaction.

$$W = (R_i + R_j)\int_{R_i+R_j}^{\infty} \frac{e^{\frac{\Phi}{k_B T}}}{h^2} h \qquad (6)$$

The potential can take into account van der Waals, Columbic, and dipole−dipole interactions.

In the simulation, three cases of W are used. The first case is aggregation in the absence of the field when $W = 1$, which is the pure Brownian aggregation mechanism. The second case is the oriented attachment of two dipoles centered on the spherical quantum dots. For the oriented attachment, the dipoles are considered in a head-to-tail arrangement. The third approach takes into account the spatially averaged dipole−dipole interaction between particles. The simulation consists of several steps. Initially, a large number of particles are generated with a given size and size distribution. Although other cases are considered, in this study the size and size distribution of the particles correspond to those of the experimentally observed magic-sized CdTe nanoparticles (Figure 3). In the simulation, the actual size and size distribution of the particles are slightly different from those determined from TEM measurments. The sizes used in this article are determined on the basis of the sizing curve of CdTe quantum dots because correlation is sought between the optical measurement and the simulation. In the following step, the evolution of the distribution is calculated in the same manner as described previously. Subsequently, the size distribution of the particles is modified by the aggregation rate. The parameters used in the simulation presented here are shown in Table 1.

Simulation Results. Figure 5a−e shows the results of the simulations. Each subfigure shows the evolution of the particle distribution versus time. The sizes of the particles are expressed in terms of particle volume (nm^3) and wavelength of absorption. The absorption wavelength is derived from the experimentally determined sizing curve for CdTe nanoparticles.[22] The particle population is expressed on a log scale to enhance the population of the larger nanoparticles. Although there is no theoretical justification for using a log scale, it is well known that the particle absorption cross section scales with increasing nanoparticle size. Because of a lack of knowledge of some of the simulation parameters, the simulation intends only to seek qualitative agreement with the experiment. The dashed lines on the right indicate the experimentally observed sizes of CdTe nanoparticles. Surprisingly, the positions of the absorption peaks remain very close in each experiments even if the experimental parameters are varied widely (different ratios of TOPO/HDA, temperature 240−270 °C, changing length of the amine).

Figure 5a shows the evolution of particles in the absence of aggregation and in the case of high initial monomer concentration. The nanoparticle distribution quickly evolves to a larger size; meanwhile, the size distribution of the particles decreases as a result of focusing effects. In the final stage of the simulation, the free monomer concentration drops to close to the solubility of the monomer ($S \approx 1$) from the initially supersaturated solution ($S_{\text{initial}} = 900$). Once all of the monomers are used, no appreciable growth occurs; only Ostwald ripening occurs, resulting in an increase in the size distribution. The experiments suggest that the positions of the absorption peaks corresponding to nanoparticle sizes do not show appreciable changes once they are formed. For this reason, Figure 5b describes a more reasonable condition when the supersaturation is much smaller ($S_{\text{initial}} = 10$); therefore, the rate of change of the particle size distribution and the average size is smaller. In this Figure, the nanoparticle distribution slightly increases, but the average size stays approximately constant. The slight broadening of the size distribution is a direct result of Ostwald ripening. The relatively slow change in the size distribution is due to how the rate-of-change curve overlaps with the particle size distribution used in the experiments.

Figure 5 c−e represents the data obtained when aggregation is turned on in the simulations. As described previously, the supersaturation of the monomer is chosen arbitrarily to be a relatively low value ($S = 10$). The subsequent peaks in the graph correspond to the volume changes induced by the aggregation of the nanoparticles. If the particle distribution is neglected, then the corresponding volume of each peak is an integer times the volume of the magic-sized particles. As mentioned above, three cases considered here are the Brownian aggregation (Figure 5c), the oriented attachment (head to tail) of dipoles (Figure 5d), and the average attraction between randomly oriented dipoles (Figure 5e). The magnitude of the dipoles is set uniformly at 100 D, which seems to be in good agreement with literature values.[32] The data from Figure 5c−e are different in two ways. First, the rate of aggregation is increased. At the same time, the appearance of the larger aggregates is faster. This is an expected result based on the basic assumption of the model. The increased aggregation rate of the smaller particles from dipoles is from a relatively small W (increased collision frequency) from eq 5. The dipole−dipole interactions also change the shape of the individual size distributions because to the left and right of the distribution of particles there will be modified rates of aggregation relative to the one predicted from the simple Brownian aggregation model. Although it might be interesting to evaluate the shape of the individual distributions, the large error in the experiments will not yield meaningful comparisons. More meaningful comparisons can be obtained from the analysis of the previously observed peak positions. In the previous paper, the observed room-temperature absorption peak positions are 410, 449, 491, 501, 539, and 588 nm. These peak positions consistently appear at the same wavelength even when the experimental parameters are widely varied. The corresponding radii of the CdTe nanoparticles are 1.13 (6.0), 1.185(7.0), 1.3(9.2), 1.335(10), 1.475(13.4), and 1.72(21.3) nm, respectively. The size distribution of the particles is approximately 30% of the average size from TEM measurements, and the values in parentheses indicate the volume of the nanoparticles in nm^3 Naturally, as the reaction proceeds, there are more peaks, but the aggregation effect is washed out and larger sizes are not clearly observable. The first peak at 1.13 nm is identified only on the basis of a room-

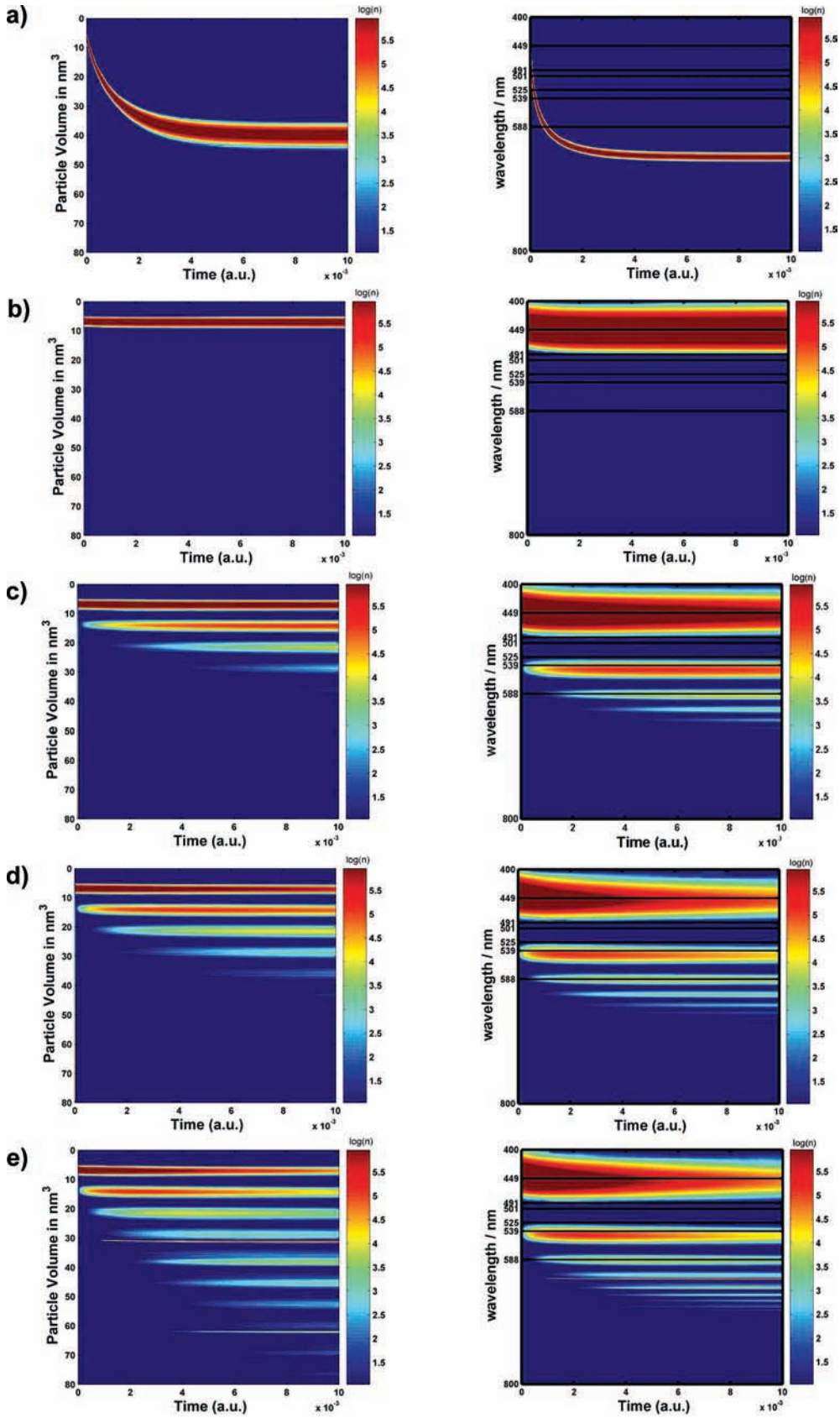

Figure 5. Simulation of the nanoparticle ensemble evolution for different conditions. The left and right graphs show the evolution particle distribution in nm^3 and wavelength, respectively. (See the text.) The initial size distribution is 1.185 ± 0.03 nm, which is equal to the size distribution of the magic-sized nanoparticles. (A) $S = 900$, no aggregation; (B) $S = 10$, no aggregation; (C) $S = 10$, Brownian-type aggregation; (D) $S = 10$, aggregation with oriented attachment; and (E) $S = 10$, aggregation with average dipole−dipole interaction potential.

temperature absorption spectrum and is related to the sizing curve. However, this peak has not been clearly identified by HRTEM. It is more likely that this peak is the secondary excitonic peak of the 1.185 nm CdTe magic-sized nanoparticles (the 449 nm peak

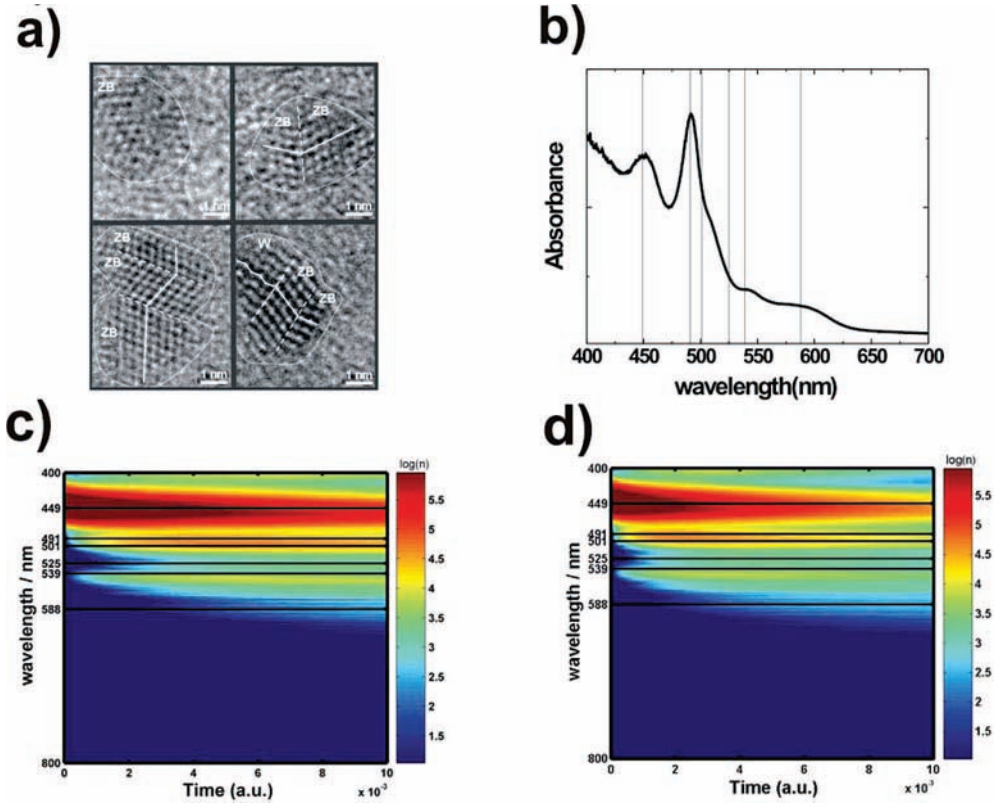

Figure 6. Simulation of the nanoparticle ensemble evolution for an initial double size distribution is 0.813 ± 0.03 and 1.185 ± 0.03 nm. (a) HRTEM images of the CdTe aggregates where the crystal phases are indicated by W and ZB corresponding to zinc blende and wurzite structures, repectively. (b) Experimental data showing the absorption peaks of the CdTe nanoparticle aggregates. The solid lines indicate the previously identified sizes. (c) $S = 10$; Brownian aggregation of the double size distribution. (d) $S = 10$; aggregation with the average dipole−dipole interaction potential.

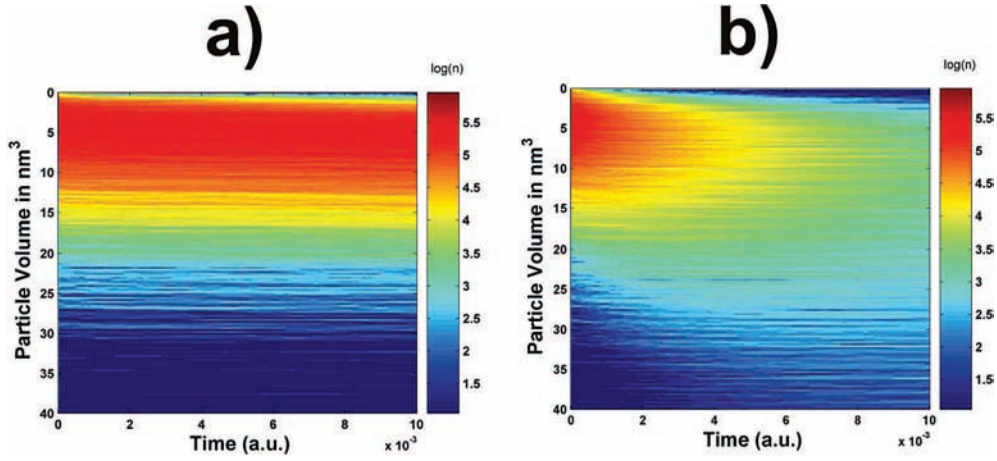

Figure 7. Simulation of the nanoparticle ensemble evolution for (A) an initial broad size distribution, which is 1.185 ± 0.3 nm. (B) $S = 10$; Brownian aggregation of the broad size distribution.

maximum in the absorption in Figure 3); therefore, it is omitted in further discussions. The experimental absorption peak positions of the various CdTe nanoparticles are indicated by dashed lines in the simulations.

The comparison of the experiment (dashed line on the simulations) and the simulation reveals that some of the sizes can be reproduced very well, but some sizes are missing. Specifically, the 539 nm ($r = 1.475$ nm or $V = 13.4$ nm^3) and the 588 nm ($r = 1.72$ nm or $V = 21.3$ nm^3) absorption peaks are well fit by the simulations (2 and 3 times the volume of the first magic size). This also means that for some sizes the volume of the magic-sized nanoparticles is an additive property, which suggests that the neck formation during nanoparticle aggregation is not significant under the experimental conditions. Interestingly, the particles corresponding to the 491 and 501 nm absorption peak positions ($r = 1.3$ and 1.335 nm) are missing from the simulation if a single magic size is initially assumed. To resolve the puzzle, a second set of simulations are carried out when the initial distribution is assumed to be a double distribution of two different magic-sized particles ($r = 1.185$ and 0.812 nm, see Figure 6a). The first magic-sized particles are kept from the first set of simulations (observed experimentally), and the second set of magic-sized particles is chosen so that the volume of the first and second set of magic-sized particles equals the volume of the particle indicated by the 491 nm absorption peak position. The comparison of the experiment

(Figure 6b) and the results from these simulations are shown in Figure 6c, d using the Brownian and average dipole-driven aggregation described above. Both of these simulations qualitatively yield similar results. The particle sizes corresponding to 491, 501, and 525 nm are reasonably well reproduced with respect to the experimental observation.

The question remains as to whether there is any rationale behind the observed second set of magic-sized CdTe nanoparticles. Although efforts have been made in our group using the MALDI technique, the particles could not be identified. Because the first magic size is relatively small and very reactive, it is speculated that the difficulty lies with the isolation of the nanoparticles (and their reactivity). This is supported by the observation of the relatively low stability of the CdTe particles. The absence of the peak from the high-temperature spectrum is not a proof of the absence of particles in the growth solution. This is especially true for very small nanoparticles, whose absorbance is skewed by the presence of the solvent and precursor absorption. It is reasonable to assume that if one magic size is observable then there might be other smaller nanoparticles. Although no direct experimental evidence is given of multiple magic sizes present, recent experiments by Manin et al.[21] have shown the presence of multiple CdSe magic-sized particles coexisting in solution. Similarly, Tonti et al.[20] reported the presence of distinct sizes of CdSe nanoparticles under selenium-rich conditions supporting the above assumption. Briefly, the conclusions of this work are that the simulation gives good agreement between experiment and theory in terms of aggregation. The simulation suggests additional magic sizes present in the growth solution. Dipole−dipole interaction increases the rate of aggregation but, to first approximation, does not change the quality and the result of the aggregation of particles.

At last, the distribution of nanoparticles is chosen to be broad initially. The results are shown in Figure 7a−c. Figure 7b indicates the evolution of the particle size distribution in the absence of aggregation and at low monomer oversaturation. The distribution becomes slightly broader, and Ostwald ripening is the dominating process. However, if the aggregation is turned on (Figure 7c), then the size distribution tends to shift to the red slightly without the presence of any distinct peaks. This situation seems to be well correlated with the experimental data presented above for the cadmium-rich condition (Figure 1a). In the case of the cadmium-rich condition, no well-defined peaks appear, and the first shoulder appears at a considerably larger size. These results suggest that even under cadmium-rich conditions there is aggregation contributing to the nanoparticle distribution. The aggregation mechanism under cadmium-rich conditions is also supported by the XRD of the final products as shown in Figure 2. Under cadmium-rich conditions, no magic size is observed; therefore, the size of crystalline domains of the larger aggregates will be smaller than under tellurium-rich conditions.

Finally, it is important to asses how the aggregation of CdTe quantum dots and the simulation carried out in this study would correlate with nanowire formation from CdTe quantum dots in an aqueous environment.[15] We believe that water would have two significant effects on the aggregation dynamics. First, the dielectric constant of water is significantly higher that those of organics, resulting in reduced particle−particle interaction. Second, redox reactions become possible, which changes the surface chemistry; therefore, the magnitude of the permanent dipole might be very different.

In conclusion, the primary reason for the observed sequential appearance of absorption peaks is due to the formation of magic-sized nanoparticles and is not due to the aggregation mechanism. The exact reproduction of data may critically depend on many parameters, but these data show qualitative agreement with the kinetics of the appearance of various nanoparticle sizes and quantitative agreement with the peak positions.

Acknowledgment. We are grateful to Kansas State University and the Department of Chemistry at Kansas State University for funding. Dr. Jacek Jasinski and the Imaging and Microscopy Facility at the University of California, Merced, are gratefully acknowledged for the use of their instruments. HRTEM studies were supported by the National Science Foundation under award number DMR-0137922.

References and Notes

(1) Shipway, A. N.; Katz, E.; Willner, I. *ChemPhysChem* **2000**, *1*, 18–52.
(2) Danek, M.; Jensen, K. F.; Murray, C. B.; Bawendi, M. G. *Chem. Mater.* **1996**, *8*, 173–180.
(3) Jin, R.; Cao, Y. C.; Hao, E.; Métraux, G. S.; Schatz, G. C.; Mirkin, C. A. *Nature* **2003**, *425*, 487–490.
(4) Talapin, D. V.; Rogach, A. L.; Haase, M.; Weller, H. *J. Phys. Chem. B* **2001**, *105*, 12278–12285.
(5) Peng, X. G.; Wickham, J.; Alivisatos, A. P. *J. Am. Chem. Soc.* **1998**, *120*, 5343–5344.
(6) Yao, J. H.; Elder, K. R.; Guo, H.; Grant, M. *Phys. Rev. B* **1993**, *47*, 14110–14125.
(7) Tu, H.; Yang, S.; Chikan, V.; Kelley, D. F. *J. Phys. Chem. B* **2004**, *108*, 4701–4710.
(8) Kalsin, A. M.; Pinchuk, A. O.; Smoukov, S. K.; Paszewski, M.; Schatz, G. C.; Grzybowski, B. A. *Nano Lett.* **2006**, *6*, 1896–1903.
(9) Bishop, K. J. M.; Grzybowski, B. A. *ChemPhysChem* **2007**, *8*, 2171–2176.
(10) Harrisson, S.; Wooley, K. L. *Chem. Commun.* **2005**, 3259–3261.
(11) Wu, Z.-S.; Guo, M.-M.; Shen, G.-L.; Yu, R.-Q. *Anal. Bioanal. Chem.* **2007**, *387*, 2623–2626.
(12) Tang, Z. Y.; Kotov, N. A.; Giersig, M. *Science* **2002**, *297*, 237–240.
(13) Shanbhag, S.; Kotov, N. A. *J. Phys. Chem. B* **2006**, *110*, 12211–12217.
(14) Ethayaraja, M.; Bandyopadhyaya, R. *Langmuir* **2007**, *23*, 6418–6423.
(15) Tang, Z.; Zhang, Z.; Wang, Y.; Glotzer, S. C.; Kotov, N. A. *Science* **2006**, *314*, 274–278.
(16) Yong, K. T.; Sahoo, Y.; Zeng, H.; Swihart, M. T.; Minter, J. R.; Prasad, P. N. *Chem. Mater.* **2007**, *19*, 4108–4110.
(17) Cho, K. S.; Talapin, D. V.; Gaschler, W.; Murray, C. B. *J. Am. Chem. Soc.* **2005**, *127*, 7140–7147.
(18) Caudia Pacholski, A. K. H. W. *Angew. Chem., Int. Ed.* **2002**, *41*, 1188–1191.
(19) Yu, J. H.; Joo, J.; Park, H. M.; Baik, S. I.; Kim, Y. W.; Kim, S. C.; Hyeon, T. *J. Am. Chem. Soc.* **2005**, *127*, 5662–5670.
(20) Tonti, D.; Mohammed, M. B.; Al-Salman, A.; Pattison, P.; Chergui, M. *Chem. Mater.* **2008**, *20*, 1331–1339.
(21) Kudera, S.; Zanella, M.; Giannini, C.; Rizzo, A.; Li, Y. Q.; Gigli, G.; Cingolani, R.; Ciccarella, G.; Spahl, W.; Parak, W. J.; Manna, L. *Adv. Mater.* **2007**, *19*, 548.
(22) Dagtepe, P.; Chikan, V.; Jasinski, J.; Leppert, V. J. *J. Phys. Chem. C* **2007**, *111*, 14977–14983.
(23) Rockenberger, J.; Tröger, L.; Rogach, A. L. *J. Chem. Phys.* **1998**, *108*, 7807.
(24) Boyen, H. G.; Kastle, G.; Weigl, F.; Koslowski, B.; Dietrich, C.; Ziemann, P.; Spatz, J. P.; Riethmuller, S.; Hartmann, C.; Moller, M.; Schmid, G.; Garnier, M. G.; Oelhafen, P. *Science* **2002**, *297*, 1533–1536.
(25) Leff, D. V.; Ohara, P. C.; Heath, J. R.; Gelbart, W. M. *J. Phys. Chem.* **1995**, *99*, 7036–7041.
(26) Stoeva, S.; Klabunde, K. J.; Sorensen, C. M.; Dragieva, I. *J. Am. Chem. Soc.* **2002**, *124*, 2305–2311.
(27) Deng, D. W.; Qin, Y. B.; Yang, X.; Yu, J. S.; Pan, Y. *J. Cryst. Growth.* **2006**, *296*, 141–149.
(28) Leff, D. V.; Ohara, P. C.; Heath, J. R.; Gelbart, W. M. *J. Phys. Chem.* **1995**, *99*, 7036–7041.
(29) Chikan, V.; Kelley, D. F. *J. Phys. Chem. B* **2002**, *106*, 3794–3804.
(30) Friedlander, S. K. *Smoke, Dust, and Haze: Fundamentals of Aerosol Dynamics*; Oxford University Press: New York, 2000.
(31) Ethayaraja, M.; Bandyopadhyaya, R. *Langmuir* **2007**, *23*, 6418–6423.
(32) Shanbhag, S.; Kotov, N. A. *J. Phys. Chem. B* **2006**, *110*, 12211–12217.

JP802254N